ABSTRACT

Title: DISCHARGE CHARACTERISTICS OF CANONICAL SPRINKLER SPRAYS

Andrew F. Blum, Master of Science, 2007

Directed By: Andre Marshall, Assistant Professor, Department of Fire Protection Engineering

Detailed characterization of spray behavior and its relationship to nozzle geometry, fluid properties, and injection characteristics is needed to advance water-based suppression technology and fire related computational fluid dynamics (CFD) tools. In this study, a series of experiments have been conducted to measure discharge characteristics of sprays produced by basic injector configurations modeled after conventional pendant sprinklers. Liquid jets of various sizes were injected downwards onto flat deflectors, tined deflectors, and boss-modified tined deflectors to establish the three canonical configurations explored in this study. Spray measurements including the initial angle of the sheet at the deflector exit, the sheet breakup radius, the drop size distribution 1 m below the deflector surface, and the volume density distribution were performed for these configurations. These systematic experiments provide discharge characteristics of practical interest while providing valuable data for CFD based atomization model development.

DISCHARGE CHARACTERISTICS OF CANONICAL SPRINKLER SPRAYS

By

Andrew F. Blum

Thesis submitted to the Faculty of the Graduate School of the
University of Maryland, College Park, in partial fulfillment
of the requirements for the degree of
Master of Science
2007

Advisory Committee:
Professor Dr. Andre Marshall, Chair
Professor Dr. Arnaud Trouve
Professor Dr. James Milke

Acknowledgements

This work is supported by the National Fire Sprinkler Association (NFSA). I want to thank the NFSA program manager Mr. Russell Fleming for his support of the project. I want to express my appreciation to Dr. Andre Marshall, my advisor, for his helpful guidance, support and the tireless hours he spent with me in the lab working on my research.

I would also like to thank the rest of my thesis committee, Dr. Arnaud Trouve and Dr. James Milke, for their guidance through this process. In addition, I would like to thank the Maryland Fire Rescue Institute for their support and facilities for my research, most notably Marty LePore and Scott Wood.

I also want to thank the rest of the Fire Protection Engineering staff at the University of Maryland for passing along their many years of knowledge to me and, as well as my fellow students that worked with me throughout my years, most notably Ning Ren, for his help with my research.

Finally, I would like to thank my girlfriend, Leigh Stewart, for her continuous support throughout the completion of my research. I could not have done it without your love and encouragement.

Table of Contents

Acknowledgements ii

Table of Contents iii

List of Figures v

Nomenclature vi

Chapter 1: Introduction 1

1.1 Overview 1

1.2 Literature Review 2

1.2.1 Sheet Disintegration Studies 2

1.2.2 Drop Size Measurements 4

1.3 Research Objectives 6

Chapter 2: Approach 8

2.1 Atomization Physics 8

2.2 Atomization Measurements 9

2.3 Diagnostics 11

2.3.1 Sheet Trajectory 11

2.3.2 Sheet Breakup 13

2.3.3 Volume Density 15

2.3.4 Drop Size 17

Chapter 3: Results and Discussion 21

3.1 Sheet Trajectory 21

3.2 Sheet Breakup 23

3.3 Volume Density 25

3.4 Drop Size Distributions.....26

Chapter 4: Conclusions.....33

List of Figures

Figure 1. Previous drop size measurements....6

Figure 2. Theoretical sheet breakup processes....9

Figure 3. The anatomy of a sprinkler....10

Figure 4. Sheet trajectory and sheet breakup diagnostic set-up....13

Figure 5. An inverted PLIF photo of the Standard nozzle at 2.07 bar....14

Figure 6. Sheet breakup photo from above the spray of the Basis nozzle....15

Figure 7. MFRI facility plan view and diagnostics....16

Figure 8. Malvern diffraction technique....18

Figure 9. Malvern drop size limitations....20

Figure 10. Initial angle results....21

Figure 11. Inverted PLIF images at radial locations within the spray....23

Figure 12. Dimensionless sheet breakup distances....24

Figure 13. Dimensionless linear density results....27

Figure 14. Local d_{v50} measurements....28

Figure 15. Rosin-Rammler/log-normal distributions....29

Figure 16. Dimensionless drop size results....32

Figure 17. Dimensionless drop size results for spaces and tines....32

Nomenclature

CVF	Cumulative volume fraction
d	Drop diameter, μm
d_{10}	Average mean drop diameter, μm
d_{30}	Average mean volume drop diameter, μm
d_{v50}	Characteristic drop diameter, μm
D_{boss}	Boss diameter, mm
D_{def}	Deflector diameter, mm
D_{inlet}	Nozzle inlet diameter, mm
D_o	Orifice diameter, mm
g	Gravitational acceleration constant, m/s^2
h	Measurement elevation, m
L_{inlet}	Length of nozzle inlet, mm
L_{jet}	Length of jet before deflector impact, mm
q'	Linear volume density
q	Measured volume flux, kg/sm^2
Q	Volumetric flow rate, lpm
QF	Volume flux fraction
r	Radius, m
r'	Non-dimensional radial coordinate (r/R)
r_{bu},	Sheet breakup distance, mm
R	Characteristic dispersion length scale, m

Re	Reynolds number
U_{jet}	Jet velocity, m/s
$(v_o)_r$	Initial radial sheet velocity, m/s
$(v_o)_z$	Initial vertical sheet velocity, m/s
VF	Spatial volume fraction
w	Rosin-Rammler/log-normal correlation coefficient
We	Weber number
x	Coordinate
y	Coordinate
z	Coordinate

Greek letters

σ	Surface tension, N/m
θ_{boss}	Angle of deflector boss, º
θ_{space}	Angle of deflector space, º
θ_{tine}	Angle of deflector tine, º
ρ	Density, kg/m^3

Subscripts

i	Drop size bin
j	Measurement station
l	Water liquid
T	Total volume

Chapter 1: Introduction

1.1 Overview

Sprinkler systems have been used to suppress fires for over a hundred years. The extinguishing ability of water and the physical mechanisms of water-based suppression are well understood. Those mechanisms include, heat extraction from the fire via drop vaporization and expansion, attenuation of heat feedback via absorption and scattering of thermal radiation, and surface cooling by drop-wise wetting. These mechanisms, along with other water-based fire suppression topics, were discussed in a comprehensive review by Grant, et al. [1].

Despite the extensive use of sprinklers, little attention has been given to atomization and spray dispersion processes. Although several experimental studies have been conducted to characterize drop size, mass flux, and velocity distributions from sprinklers, this research has not been fully utilized to formulate physical models characterizing the initial spray characteristics and their relationship to sprinkler geometry [2-10]. The absence of atomization models for sprinklers continue to result in large uncertainties in the specification of initial spray characteristics essential for computer simulations of water-based suppression design and analysis.

Atomization physics indicate that intermediate processes, including sheet formation and disintegration, affect the spray characteristics before drops are formed [11-20]. Therefore it is important to investigate the sheet breakup dynamics of the initial spray in order to gain insight into sprinkler discharge characteristics. The current study focuses on establishing relationships between discharge characteristics and critical

geometric features common to most sprinklers through carefully conceived experiments centered on sprinkler geometry, sheet breakup dynamics, volume flux, and initial drop size.

1.2 Literature Review

Sprinklers typically use an impinging jet configuration where water is supplied to a fire by injecting a continuous liquid stream onto a deflector, forming a radially expanding sheet that disintegrates and disperses water in the form of drops. When studying the atomization and dispersion processes of a sprinkler, several physical mechanisms contribute to the atomization process governing the initial spray and its subsequent dispersion. These atomization processes have been studied extensively for a variety of liquid injection devices. A few atomization studies are summarized in the following section, including those specifically focused on sprinkler sprays.

1.2.1 Sheet Disintegration Studies

Dombrowski, et al. conducted a series of seminal studies exploring the physics of liquid sheet atomization [12-14]. The experiments in these studies typically involved small fan nozzles employed to create flat, wavy liquid sheets at pressures ranging from 0.21-3.45 bar. The sheets were visualized using a high-speed flash photography technique providing high contrast images of a bright, liquid sheet with a dark, black background. These studies characterized the aerodynamic wave motion on high-velocity sheets and provided analysis for determination sheet breakup and ultimately drop size based on wave instability concepts.

Huang investigated the breakup radius of axisymmetric sheets formed by the impingement of two co-axial jets by exploiting a photographic technique similar to Dombrowski [15]. Huang determined a semi-empirical correlation for liquid sheets in ambient air, relating the dimensionless sheet breakup radius, $2r_{bu}/D_o$, to the Weber number at conditions having $800 < We < 40{,}000$. The breakup radius, r_{bu}, and the orifice diameter, D_o, describes the dimensionless breakup location while the Weber number is defined as the ratio of the inertial forces divided by the surface tension forces, $We = \rho_l U^2 D_o / \sigma$ [21]. The liquid density, ρ_l, jet velocity U_{jet}, and orifice diameter describe the inertial forces and surface tension effects are represented by σ. Scaling the sheet breakup distance with the Weber number was first performed by Ostrach & Koestel, who determined the dimensionless breakup distance scaled with $1/We$ for Weber numbers greater than 10,000, an obvious divergence between the experimental results of Huang [20].

Prahl and Wendt conducted a series of experiments to determine breakup locations of a sheet generated by a jet impinging on a flat disk [17]. In these moderate Weber number experiments having $1600 < We < 4000$, controlled disturbances were created using a vibrating deflector. The critical, or most unstable, wavelength was determined by finding the forcing frequency (and corresponding wavelength) that provided the earliest breakup determined by high-speed photography. These sheet breakup location measurements also demonstrated the $We^{-1/3}$ scaling law proposed by Huang.

More recently, Clanet and Villermaux measured sheet breakup for smooth and flapping sheets in an impinging jet configuration using laser induced fluorescence in conjunction with short exposure, high-speed photography [18-19]. They established that

the smooth, or steady, sheet transitions to a flapping, unsteady sheet at a critical Weber number of 1200. Once this critical Weber number is exceeded, the dimensionless sheet breakup, $2r_{bu}/D_o$, follows a $We^{-1/3}$ scaling law. Both of these conclusions mirror the results established by Huang when describing the different sheet breakup regimes and the Weber number scaling laws.

1.2.2 Drop Size Measurements

Classical sprinkler experiments were conducted by Dundas where drop size measurements were performed for six sprinkler configurations with orifice diameters ranging from 3.1 - 25.4 mm over a wide range of pressures, 0.345 – 5.52 bar [2]. A high speed flash photography technique was applied to measure droplets in the initial breakup region, 0.61 meters from the sprinkler centerline, which involved a tedious photographic drop counting method. Dundas concluded that the dimensionless characteristic drop size, d_{v50}/D_o, follows a $We^{-1/3}$ scaling law. The dimensionless characteristic drop size, d_{v50}/D_o, from Dundas and others is provided in Figure 1.

Yu performed drop size measurements for 16.3 mm, 13.5 mm, and 12.7 mm diameter upright sprinklers at radial locations spanning the entire spray, 3 and 6 meters below the head [3]. A laser-based imaging technique for measuring drop size was adopted for these experiments, which had previously been used for measurements inside of rain clouds. Yu's results for one sprinkler, operated at two pressures, followed the $We^{-1/3}$ scaling law first observed by Dundas, and have been included in Figure 1.

More recently, Widmann measured discharge characteristics of four residential sprinklers with orifice diameters of 8.0 – 11.0 mm, operated at pressures 0.69 – 2.0 bar [4-6]. A Phase Doppler Interferometer (PDI) was used to measure the drop size and

velocity at radial locations approximately 1 m below the sprinkler head. The main objective of the study was to validate the PDI technique, not the drop size dependence on Weber number, therefore only one sprinkler was investigated for a Weber number dependency. Widmann's measurement of the average mean volume diameter, d_{30}, shown in Figure 1, demonstrates the $We^{-1/3}$ dependence, except at low pressures, 0.69 bar.

Clanet and Villermaux measured drop sizes for a jet impinging onto a disk while conducting their laser induced fluorescence experiments [19]. The drop size, an average value denoted as d_{10}, appears to hit a minimum value at large Weber numbers having $3000 < We < 30{,}000$, as depicted in Figure 1.

Sheppard performed a series of extensive initial spray experiments testing over 16 common residential sprinklers, both pendent and upright, for drop size, velocity, and trajectory [7-8]. The sprinklers varied in orifice size from 9.5 - 25.4 mm and were operated at pressures of 0.345 – 5.52 bar. The drop sizes were determined by the PDI technique perfected by Widmann, at various circumferential and azimuthal angles within the initial spray, either 0.38 or 0.61 m from the sprinkler centerline. A local characteristic drop size, d_{v50}, was determined at each location and is provided n Figure 1. However, the drop size trend with respect to Weber number was difficult to evaluate because an overall drop size for the entire spray was not available; only the local measurements were provided.

Putorti applied a Particle Tracking Velocimetry and Imaging (PTVI) technique, which is a laser-based fluorescence technique, to measure drop size, velocity, trajectory, and mass flux [9-10]. The nozzles consisted of a jet impinging onto conical sprinkler plates at angles of 60º, 90º, and 120º, and orifice diameters ranging from 4.0 – 8.5 mm

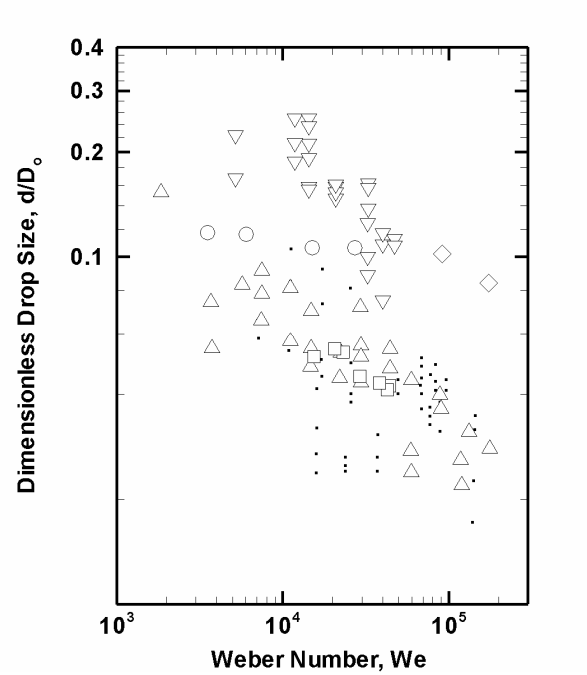

Figure 1. Previous drop size measurements: △ Dundas (d_{v50}); ◇ Yu (d_{v50}); □ Widmann (d_{30}); • Sheppard (local d_{v50}); ▽ Putorti (d_{v50}); ○ Clanet & Villermaux (d_{10}).

operated at pressures between 0.21 and 4.34 bar. Putorti observed a characteristic drop size, d_{v50}, dependence of $We^{-2/3}$ and his measurements are presented in Figure 1.

1.3 Research Objectives

The primary purpose of this study is to provide measurements of discharge characteristics in canonical sprinkler configurations. The critical discharge characteristics of interest are the drop size, velocity, and location distributions describing the spray. These measurements will provide a foundation for physics-based atomization models to be used for sprinkler design and CFD analysis.

As demonstrated in Figure 1, there is a wide range of drop size measurements that have already been conducted for various sprinkler geometries by a variety of experimental techniques. This wide range of drop size measurements is not ideal for the

purposes of model development and validation. Therefore, a second objective of this study is to conduct several careful experiments that yield reproducible and dependable results for model development.

Chapter 2: Approach

Historically, the most sought after quantity in sprinkler sprays has been the drop size, as this quantity closely affects the penetration cooling and oxygen displacement performance of the spray. Characterizing the drop size is the principal focus of this study; however, an understanding of atomization physics suggests there are important intermediate processes that govern the drop formation. In this study, these intermediate processes are characterized through a series of careful experiments for canonical sprinkler configurations. This approach will provide insight into the atomization physics and generate valuable data to support development and validation of a parallel modeling study.

2.1 Atomization Physics

The atomization process for low and medium pressure sprinklers can be described by three distinct stages, as illustrated in Figure 2. The injector forms a vertical water jet that impinges upon a striker plate, or boss. The redirected jet forms a thin, horizontal film traveling along the top of the deflector. Once the film travels past the deflector, it transforms into an unconfined, expanding sheet. The sheet expands radially outwards from the deflector becoming increasingly unstable, creating aerodynamic waves. These sinuous waves grow until the sheet begins to breakup at a critical wave amplitude. The sheet disintegrates into ring-like ligaments that are also inherently unstable. Dilatational waves grow on the ligament until they reach a critical wave amplitude, initiating ligament breakup into smaller water fragments. These fragments will eventually contract to form

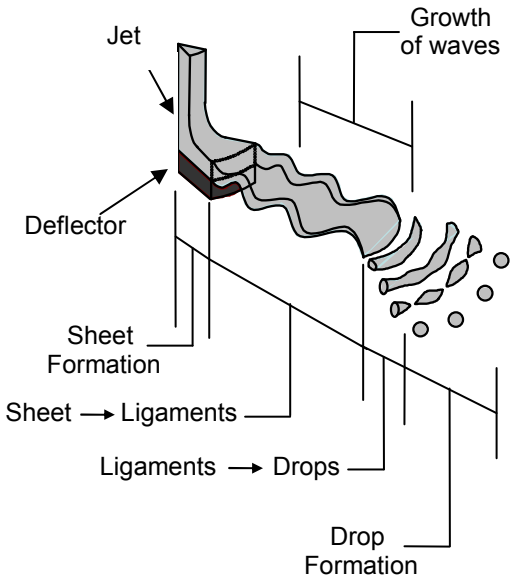

Figure 2. Theoretical sheet break up processes [22].

spherical water drops. A more detailed discussion of atomization processes along with the stages of sheet formation and disintegration can be found in Wu [23] and Lefebvre [24].

2.2 Atomization Measurements

When dissected and studied in great detail, the anatomy of a sprinkler is a complex configuration that needs to be characterized carefully to ensure each geometric characteristic is represented accurately. Figure 3 depicts the sprinklers investigated in this study as well as the important geometric characteristics common to most sprinklers.

In this study, three different canonical sprinkler configurations were investigated, identified as the Basis, Tined, and Standard nozzles. The Basis nozzle consists of a separate injector and deflector disk. It does not have tines, frame arms, or a boss. This

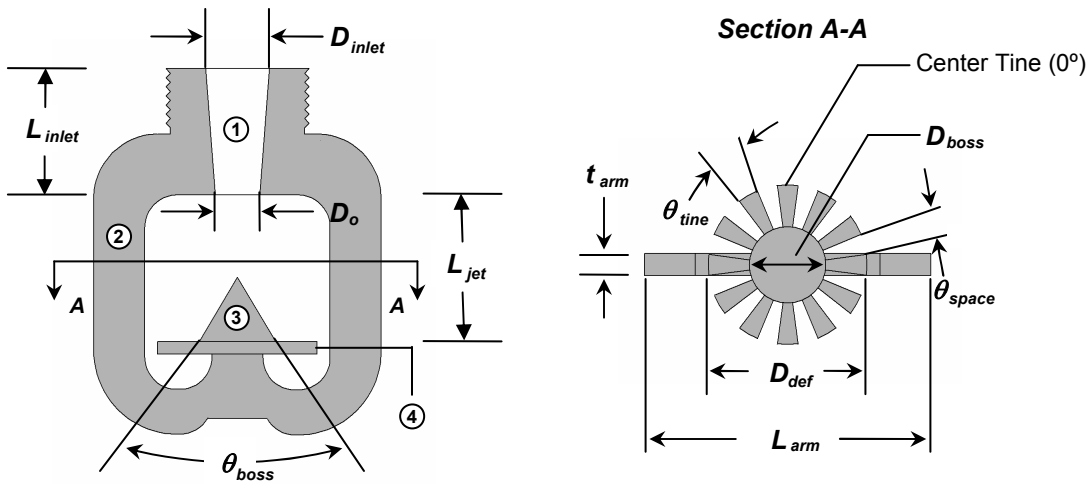

Figure 3. The anatomy of a sprinkler: (1) Inlet (2) Frame Arms (3) Boss (4) Deflector.

canonical configuration provides a useful baseline for evaluating the impact of additional geometric features on discharge characteristics. The Tined nozzle configuration helps to isolate and explore the effect of tines and spaces on a deflector. The nozzle was fabricated by removing the conical boss from a standard Tyco D3 nozzle, leaving a flat, notched deflector. A conventional Tyco D3 nozzle was utilized for the Standard nozzle adding boss effects and extending the nozzle geometry to a commercially available configuration. Table 1 summarizes the important geometric and flow characteristics for all three nozzles used in this study.

The influence of sprinkler spray geometry on discharge characteristics is aided by measurement and analysis of intermediate processes occurring during atomization. The two intermediate processes measured in this study were sheet trajectory and sheet breakup location. These measurements provide insight into the dispersion behavior of the spray along with valuable information for atomization model validation and development. In addition to examining the intermediate processes leading to drop

Table 1. Experimental Sprinkler Dimensions

		Basis Nozzle			Tined Nozzle	Standard Nozzle
Inlet Characteristics	D_{inlet} (mm)	19	19	19	19.5	19.5
	L_{inlet} (mm)	25.4	25.4	25.4	19.7	19.7
	L_{jet} (mm)	25.4	25.4	25.4	23	23
	D_o (mm)	3.5	6.7	9.7	6.35	6.35
	K-Factor (lpm/bar$^{1/2}$)	7.2	25.9	49.0	25.9	25.9
Deflector Characteristics	D_{def} (mm)	38	38	38	25.4	25.4
	θ_{tine} (º)	None	None	None	21	21
	θ_{space} (º)	None	None	None	9	9
Boss Characteristics	D_{boss} (mm)	None	None	None	12	12
	θ_{boss} (º)	None	None	None	180	65

formation, other spray characteristics were measured including volume flux and drop size distributions along the radial extent of the spray. These detailed measurements were used to determine global spray characteristics such as the overall d_{v50}.

2.3 Diagnostics

Sheet trajectory, sheet breakup, volume density, and local drop size experiments were conducted to quantify discharge characteristics for each of the experimental nozzle configurations. The experiments were performed at 0.69, 1.38, 2.07, and 2.76 bar to investigate the effect of injection pressure on spray characteristics. Table 2 summarizes the pertinent experimental injection parameters including injection pressure, P, jet velocity, U_{jet}, nozzle flow rate, Q, Weber number, We, and Reynolds number, Re, where the Weber and Reynolds numbers are based upon the jet velocity.

2.3.1 Sheet Trajectory

Sheet trajectory experiments were conducted to track the path of the radially

Table 2. Experimental Injection Parameters

	D_{inlet} (mm)	ΔP (bar)	U_{jet} (m/s)	Q (lpm)	*We*	*Re*
Basis Nozzle	D_o = 3.5	0.69	11.8	1.6	6509	41059
		1.38	16.6	2.2	13019	58066
		2.07	20.4	2.7	19528	71116
		2.76	23.5	3.2	26038	82118
	D_o = 6.7	0.69	11.8	5.7	12461	78598
		1.38	16.6	8.0	24922	111155
		2.07	20.4	9.9	37383	136136
		2.76	23.5	11.4	49844	157197
	D_o = 9.7	0.69	11.8	10.8	18041	113792
		1.38	16.6	15.2	36081	160926
		2.07	20.4	18.6	54122	197093
		2.76	23.5	21.5	72162	227583
Tined Nozzle	D_o = 6.35	0.69	11.8	5.7	11810	74493
		1.38	16.6	8.0	23620	105348
		2.07	20.4	9.9	35430	129025
		2.76	23.5	11.4	47240	148985
Standard Nozzle	D_o = 6.35	0.69	11.8	5.7	11810	74493
		1.38	16.6	8.0	23620	105348
		2.07	20.4	9.9	35430	129025
		2.76	23.5	11.4	47240	148985

expanding sheet beyond the edge of the deflector. The experiments were conducted inside a vented 1.7 m x 1.7 m x 1.9 m chamber illustrated in Figure 4. Planar Laser Induced Fluorescence (PLIF) was utilized to visualize a cross-section of the expanding sheet. Illumination was provided by a 500 MW, air cooled, argon ion laser and a 20 face rotating mirror spinning at 20 Hz. The water supply was seeded with a rhodamine 6G dye having a mass concentration of 0.5 mg/l. The sheet was imaged with a low noise, 16-bit, 2.0 mega-pixel, Cooke SE © high-speed digital video camera fitted with a high pass optical filter operated with an electronic shutter speed of 900 μs at 5 frames per second. Comparison of several images at each flow condition revealed that the trajectory, before

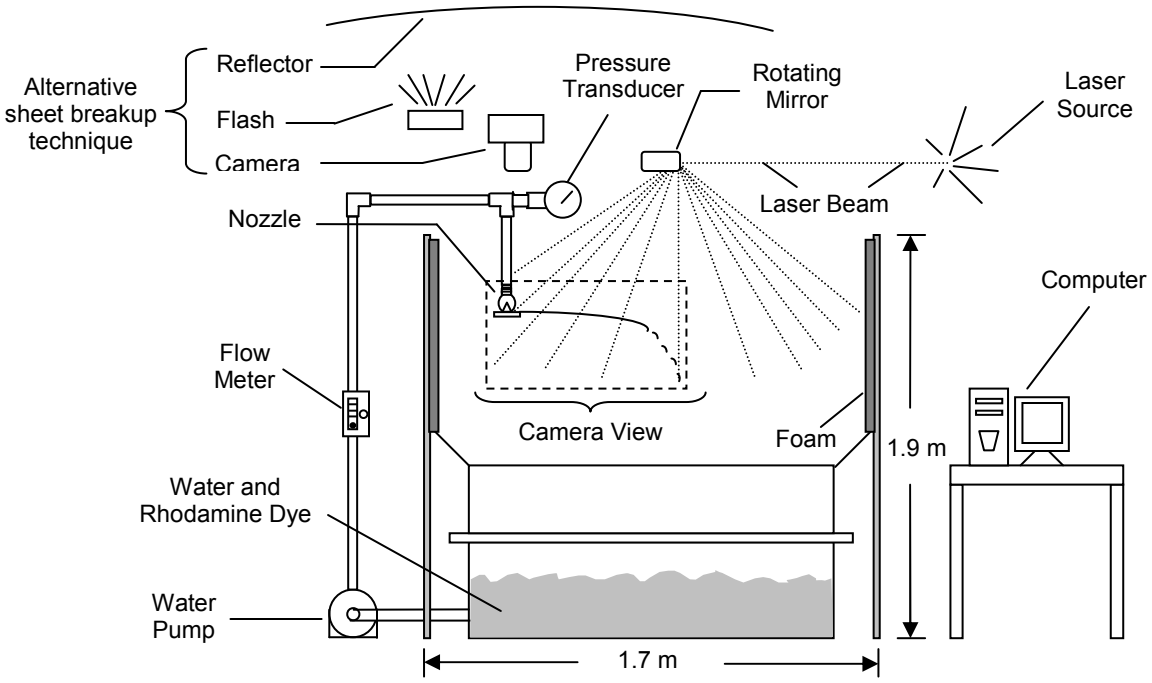

Figure 4. Sheet trajectory and sheet breakup diagnostic set-up.

breakup, is essentially time-independent. A single image was thus used along with a spatial calibration for determination of the sheet trajectory as shown in Figure 5.

2.3.2 Sheet Breakup

The PLIF technique described previously also provides images for determining the radial location where the flapping, wavy sheet breaks up completely into ligaments. The PLIF image shown in Figure 5 is also representative of those used to determine the breakup distance, where the breakup distance was defined as the location where the continuous sheet no longer exists and only ligaments remain. At least 100 images were analyzed at each experimental condition to ensure statistically steady results. However, the PLIF technique did not provide satisfactory results for very thin sheets with long

Figure 5. An inverted PLIF photo of the Standard nozzle at 2.07 bar.

breakup distances, such as those produced by the smallest Basis nozzle. An alternative photographic technique was used to determine sheet breakup locations in these cases, as previously illustrated in Figure 4. In this photographic method, the sheet was illuminated with a 15.6 μs diffuse-reflected Canon 550EX flash. A Canon D30 Digital SLR camera was placed above the nozzle to photograph the sheet breakup producing images similar to the one depicted in Figure 6. Where, once again, the breakup distance was defined as the location where the sheet is completely broken up into ligaments. At least 10 images were recorded at each experimental condition and multiple breakup locations were obtained at circumferential stations distributed around the sheet. This alternative technique was used for all Basis nozzle breakup measurements because they produced thin, long sheets (especially the smallest nozzle). On the other hand, the Tined and Standard nozzles were determined by the PLIF technique because the complexities of their sprays resulted in indecipherable images using the alternative technique. Comparisons of the breakup locations for the 6.7 mm Basis nozzle, using both photographic techniques, showed agreement within 12.8%, verifying that both techniques can effectively determine the breakup distance.

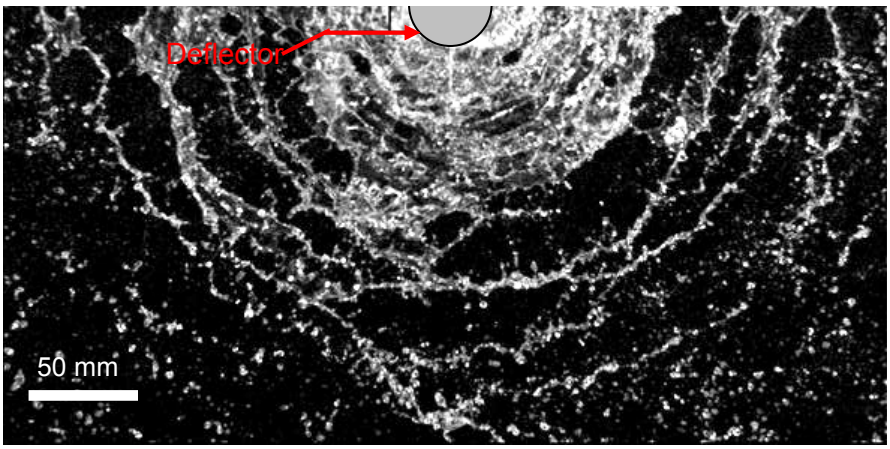

Figure 6. Characteristic sheet breakup photo from above the spray [22].

2.3.3 Volume Density

Knowledge of the volume distribution dispersed onto the floor is helpful in model development as well as critical to the determination of the overall characteristic drop size, d_{v50}, described later. Volume density distributions were obtained using a 2.6 m patternator positioned 1 m below the nozzle deflector surface and 1 m above the floor. To permit analysis of the entire sprinkler spray, volume density measurements were conducted inside a large 8.6 m x 7.2 m x 3 m room located at the Maryland Fire Rescue Institute, as illustrated in Figure 7. The nozzles were discharged for 10 minutes to average over short time scale aerodynamic or water supply fluctuations, after which the water in each cup was weighed to determine the volume at each radial station. After verifying the axisymmetry and repeatability of the Basis nozzle spray at 0º and 30º stations (± 2%), radial volume density distributions were obtained only at the 0º station. Meanwhile, the Tined and Standard nozzles were tested at the 0º and 15º stations. These stations were aligned with the middle of the center tine and adjacent space, respectively, as illustrated in Figure 2.

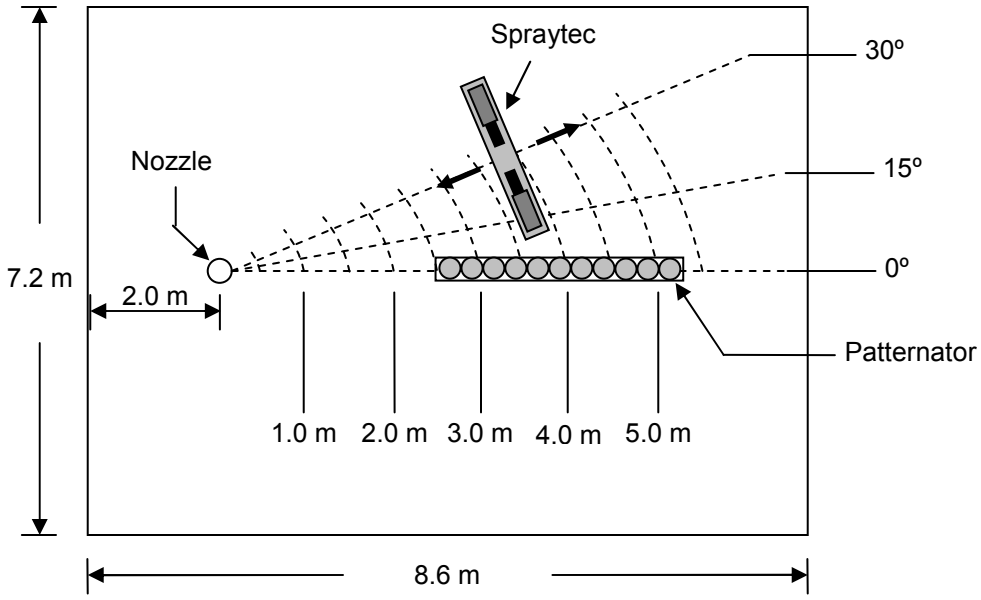

Figure 7. MFRI facility plan view and diagnostics.

A characteristic dispersion length scale, R, first introduced by Prahl and Wendt [17], was employed to facilitate analysis of the measurements. This reference quantity provides an inviscid radial location at the measurement elevation for each experimental condition, and is given by

$$R = (v_o)_r \left(\frac{2h}{g}\right)^{1/2} \left[\left(1 + \frac{(v_o)_z^{\,2}}{2gh}\right)^{1/2} - \left(\frac{(v_o)_z^{\,2}}{2gh}\right)^{1/2} \right], \qquad (2.1)$$

where h is the measurement elevation (below the nozzle), g is the gravitational constant, $(v_o)_r$ is the initial radial sheet velocity, and $(v_o)_z$ is the initial vertical sheet velocity. The velocity magnitude is estimated using a model describing viscous interaction with the deflector [25], and the angle is determined from the average initial angle at that experimental condition determined by the trajectory measurements, yielding sheet velocities $(v_o)_r$ and $(v_o)_z$. The resulting volume density distributions in the r/R coordinate

describe the relative effect of drag on dispersion. The volume density measurements were described non-dimensionally so that

$$\sum q_i' \Delta r' = 1\,, \tag{2.2}$$

where $\Delta r' = \Delta r / R$ is the dimensionless station width and the dimensionless linear density of dispersed volume flow, q_i', is given by

$$q_i' = \frac{q_i}{Q/\pi R^2}(2r'), \tag{2.3}$$

where q_i is the volume flux measured at drop size *i* and Q is the nozzle flow rate. The length scale *R* was modified at every experimental condition except at measurements aligned with spaces (15º station) for the Tined and Standard nozzles. At these measurement stations the initial angle and corresponding velocity magnitude could not be determined from the trajectory experiments described previously. For these cases, *R* values at measurement locations aligned with the tine (0º station) were used for measurement locations aligned with the space (15º station) to facilitate comparison.

2.3.4 Drop Size

Local drop size measurements were also conducted inside the large room illustrated in Figure 7 to investigate the drop size variations along the radial span of the spray. An overall drop size distribution and a characteristic drop size, d_{v50}, for each experimental condition can be derived from these measurements. The local drop sizes were measured using a Spraytec particle analyzer developed by Malvern Instruments [26]. This laser-based instrument employs a light diffraction technique for counting and sizing drops or particles. As illustrated in Figure 8, the instrument's sampling volume is created with a collimated laser diode. Drops entering this sampling volume diffract light at various

angles according to their size. This light is collected by detector rings to measure the intensity distribution. The intensity distribution is used along with proprietary correlations to calculate the drop size distribution. The entire signal is then focused onto a power detector which measures attenuation of the incident light providing an estimate of the concentration.

Local measurements were taken at 12 radial stations starting at 0.5 m and separated by 0.5 m, positioned 1 m below the nozzle and 1 m above the floor. The Spraytec measurement volume was configured to be 12 mm in diameter and 130 mm long. At least 100 drops were estimated to fill the measurement volume for valid measurement records. Measurements were taken at each station for 1 minute at 50 Hz providing local drop size distribution realizations. The drop sizes were measured at the same circumferential stations as the volume flux experiments and in the case of the Basis nozzle demonstrated similar axisymmetric behavior.

The drop size distribution determined by the Malvern RTSizer software v 5.3.1.0 is a local drop size distribution within the Spraytec's measurement volume [27].

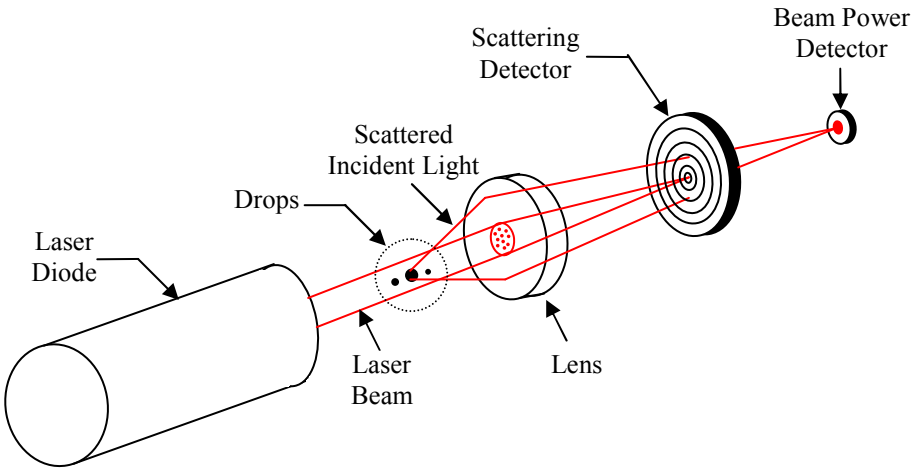

Figure 8. Malvern diffraction technique.

However, in this study an overall characteristic drop size, d_{v50}, for the entire spray is of interest. To determine the overall d_{v50} the local Spraytec measurement is weighted with the local volume density measurements to transform the spatial Malvern measurements into the flux-based drop size distributions described in equations 2.4 – 2.6.

$$Q_i = \sum_{j=1}^{N} (q'_j) \Delta r' V F_{i,j} \tag{2.4}$$

$$Q_T = \sum_{i=1}^{M} \sum_{j=1}^{N} (q'_j) \Delta r' V F_{i,j} \tag{2.5}$$

$$QF_i = Q_i / Q_T \tag{2.6}$$

where $VF_{i,j}$ is the local spatial volume fraction within the Spraytec measurement volume for the *i*th drop size at the *j*th measurement location. The spray quantities Q_i and Q_T are estimates of the drop-wise volume flux and total volume flux from all drops, respectively. The quantity QF_i is the flux-based drop-wise volume flux fraction for the entire spray. Drop size distributions based on 60 drop size bins ranging from 0.29 – 2000 μm are easily calculated from QF_i for determining flux based drop characteristics.

The upper measurement limit of the Spraytec (d_{v50} = 850 μm) presents a challenge for measuring the larger drop sizes produced by the nozzles used in this study. This limit is clearly observed in the radial drop size distribution measurements for the Basis nozzle configurations presented in Figure 9. The figure also demonstrates that under quiescent conditions, the drag effects result in reduced penetration of smaller drops in the dimensionless coordinate when compared to larger drops, regardless of the experimental

condition. However, at extreme radial locations, surprisingly drop size measurements did not change significantly with location and remained slightly below the Spraytec d_{v50} limit. The spatial separation of drops is easily predicted through drop dispersion calculations, including drag effects, for the various drops [25]. The favorable comparison between model predictions and valid Spraytec measurements, demonstrated in Figure 9, provides an opportunity to correct the erroneous drop size measurements at extreme radial locations. At these locations, drop size measurements were replaced with those from the drop dispersion model estimates. It should be noted that the contaminated region typically consisted of only 5 -15% of the total mass of the spray for the Basis and Tined nozzles and even less for the Standard nozzle, resulting in only small adjustments to the overall drop size distribution and the associated characteristic drop sizes.

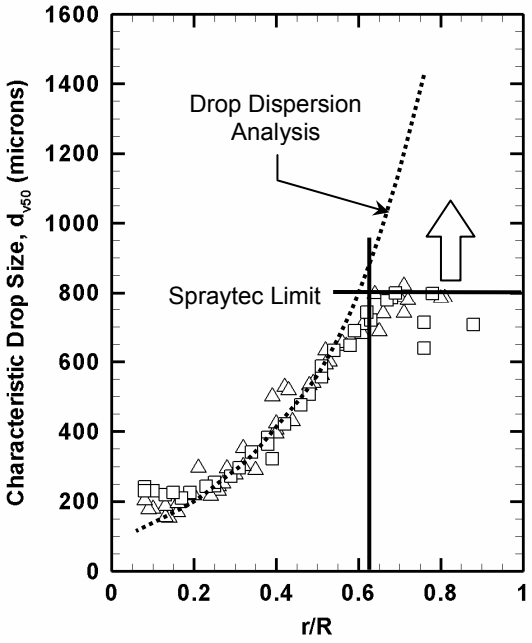

Figure 9. Malvern drop size limitations: ····· Drop Dispersion Analysis; Basis nozzle: △ D_o = 3.5 mm; ▽ D_o = 6.7 mm; □ D_o = 9.7 mm.

Chapter 3: Results and Discussion

3.1 Sheet Trajectory

The initial angle, θ, was determined for each nozzle configuration and experimental condition through analysis of the PLIF images. Trajectory measurements performed on the Basis nozzle and on the other nozzles aligned with the center of the tine (0º station) revealed that the sheet does not deviate from its initial angle. Significant curvature was only observed in the Standard nozzle operating at low pressures. The initial angle does not exhibit any consistent Weber number functionality for a given nozzle. Instead, dependence between the initial angle and orifice diameter was observed, demonstrated in Figure 10 and summarized in Table 3.

The addition of spaces on the deflector in the Tined nozzle does not have a significant

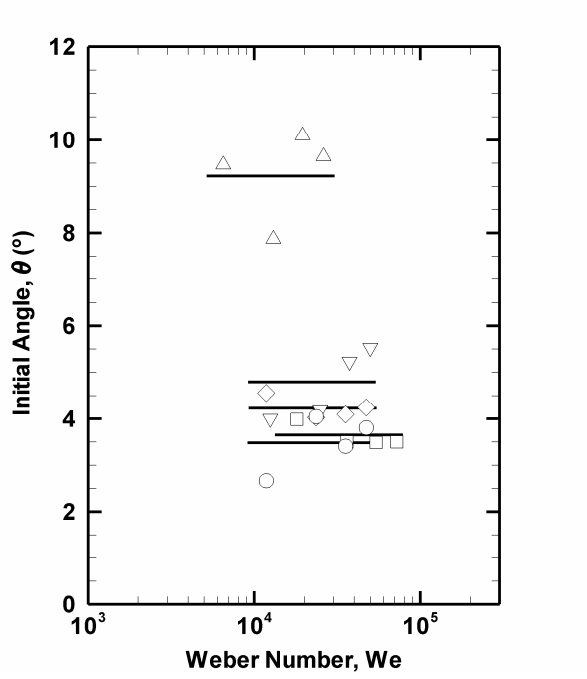

Figure 10. Sheet trajectory measurements; ——— Average Angle; Basis nozzle: △ D_o = 3.5 mm; ▽ D_o = 6.7 mm; □ D_o = 9.7 mm; Tined nozzle: ◇ D_o = 6.35 mm; Standard nozzle: ○ D_o = 6.35 mm.

effect upon the initial angle when compared to the Basis nozzle value with a similar orifice diameter. These nozzles have initial angles of 4.2º and 4.7º, respectively. However, the Standard nozzle had an average initial angle of 3.5º, which is smaller than both the Tined and Basis nozzles at approximately the same orifice diameter.

For the Tined and Standard nozzles the trajectory of the sheet exiting the tine was easy to distinguish. However, the sheet trajectory in the spaces between the tines was difficult to discern due to the limitations of the measurement equipment and complexities of the spray in the spaces. To obtain insight into the flow of water in the spaces, qualitative PLIF images were acquired in planes orthogonal to the center tine at radial locations 12.7 mm, 22.7 mm, and 62.7 mm, from the center of the deflector, as illustrated in Figure 11(a).

Table 3. Summary of Discharge Characteristics

			Basis Nozzle			Tined Nozzle		Standard Nozzle	
	ΔP (bar)	U_{jet} (m/s)	$D_o = 3.5$	$D_o = 6.7$	$D_o = 9.7$	Tine (0º)	Space (15º)	Tine (0º)	Space (15º)
Initial Angle, θ (º)	0.69	11.8	9.47	4.00	3.99	4.56	N/A	2.67	N/A
	1.38	16.6	7.87	4.19	3.50	4.03	N/A	4.05	N/A
	2.07	20.4	10.10	5.23	3.49	4.10	N/A	3.41	N/A
	2.76	23.5	9.65	5.53	3.50	4.25	N/A	3.81	N/A
Average, θ (º)	N/A	N/A	9.27	4.74	3.62	4.23	N/A	3.49	N/A
Sheet Breakup Distance, $2r_{bu}/D_o$	0.69	11.8	49.43	37.58	37.11	30.56	N/A	21.48	N/A
	1.38	16.6	39.18	31.91	33.81	29.27	N/A	17.62	N/A
	2.07	20.4	37.39	30.72	N/A	27.31	N/A	15.30	N/A
	2.76	23.5	34.64	28.72	N/A	25.87	N/A	13.46	N/A
Overall Characteristic Drop Size, d_{v50}/D_o	0.69	11.8	0.155	0.091	0.085	0.101	0.104	0.087	0.056
	1.38	16.6	0.149	0.081	0.076	0.097	0.100	0.073	0.053
	2.07	20.4	0.143	0.082	0.080	0.094	0.103	0.062	0.048
	2.76	23.5	0.146	0.081	0.074	0.089	0.101	0.059	0.045

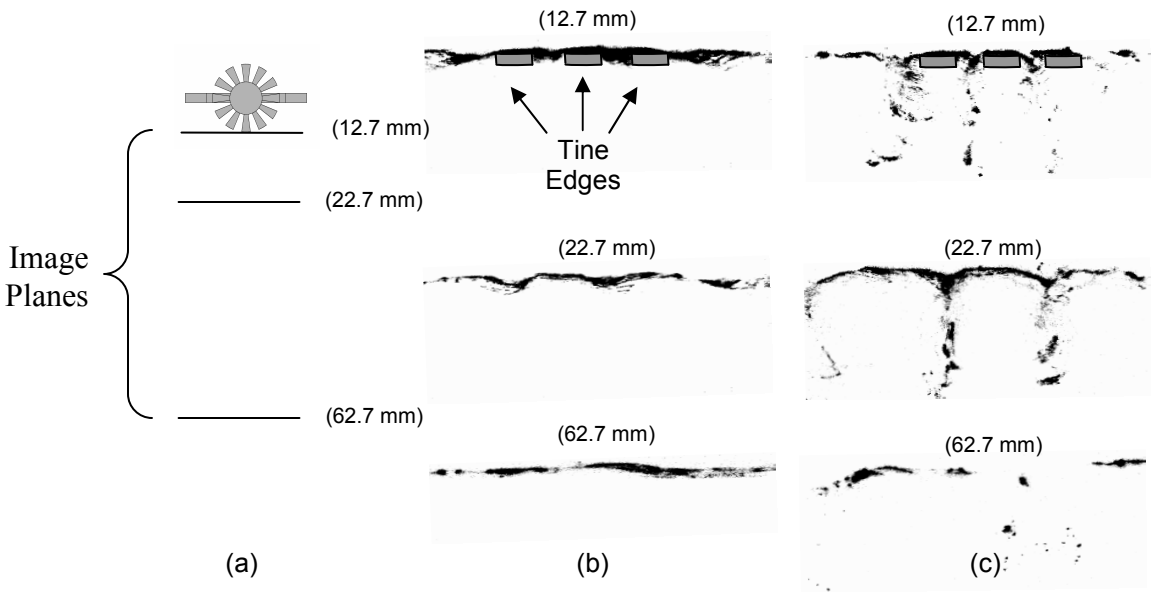

Figure 11. Inverted PLIF images depicting flow through sprinkler spaces: (a) Top view of measurement locations (b) Tined nozzle (c) Standard nozzle.

Figure 11(b) demonstrates the Tined nozzle creates a relatively flat sheet that is not significantly affected by the spaces between the tines. In contrast, the Standard nozzle, shown in Figure 11(c), appears to direct a significant amount of water through the spaces. This creates a three dimensional sheet formed by the flow over the tines and the flow forced through the spaces by the boss.

3.2 Sheet Breakup

High-speed flash photography was used to determine sheet breakup for the Basis nozzle, while a PLIF technique was employed for the more complex Tined and Standard nozzles. As described in Figure 12 and summarized in Table 3, the dimensionless sheet breakup location for each experimental condition is presented with respect to the Weber number along with data from Huang, a previous investigator who measured the

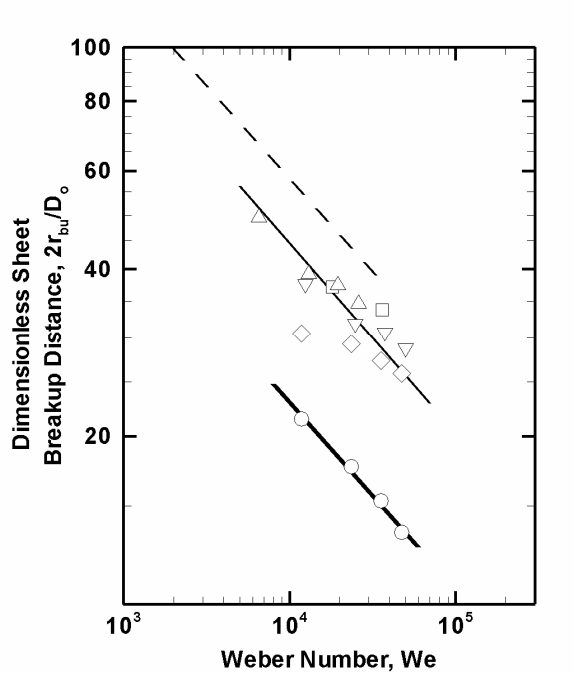

Figure 12. Dimensionless sheet breakup distances: ---- Huang Correlation; —— Basis Correlation; ━━ Standard Correlation; Basis nozzle: △ D_o = 3.5 mm; ▽ D_o = 6.7 mm; □ D_o = 9.7 mm; Tined nozzle: ◇ D_o = 6.35 m; Standard nozzle: ○ D_o = 6.35 mm.

sheet breakup distance for axisymmetric sheets [15]. Huang proposed a semi-empirical correlation for his axisymmetric sheets described as

$$2r_{bu}/D_o = 1250We^{-1/3} \tag{3.1}$$

The breakup distance of the Basis nozzle for all three orifice diameters correlates well with one another and follows the $We^{-1/3}$ scaling law proposed by Huang. This study's empirical correlation for the Basis nozzle was determined to be

$$2r_{bu}/D_o = 964We^{-1/3}, \tag{3.2}$$

which falls below the correlation determined by Huang ($2r_{bu}/D_o = 1250We^{-1/3}$). This discrepancy could be a result of differing methodologies for creating the horizontal, axisymmetric sheets. Huang used two opposed impinging jets to create his radially

expanding sheets, while a single jet impinging upon a flat deflector surface was used in this study.

Sheet breakup measurements of the Tined nozzle also follow a $We^{-1/3}$ scaling at higher pressure conditions, with the exception of the lowest pressure (0.69 bar) data point. However, the sheets created with the Tined nozzle break up sooner than that of the Basis nozzle at a similar orifice diameter. The scaling of the Tined nozzle appears to follow the $We^{-1/3}$ at higher pressure conditions, with a break down at the lowest pressure (0.69 bar), resulting in an outlaying data point. The Standard nozzle sheet breakup distances also demonstrated the $We^{-1/3}$ scaling law and were the shortest when compared to the two other configurations. The empirical correlation for Standard nozzle configuration was determined to be

$$2r_{bu}/D_o = 495We^{-1/3}, \tag{3.3}$$

breaking up at approximately one-half the distance of the Basis nozzle. From these experiments it is clear the addition of first tines and spaces, and then the boss promotes sheet instability, resulting in earlier sheet disintegration.

3.3 Volume Density

In Figure 13, results from volume distribution experiments are presented in terms of a dimensionless linear volume density, q', and a dimensionless radial location, *r/R*. The Basis nozzle presented in Figure 13(a) – (c), demonstrates the effect of increasing the orifice diameter. As the orifice diameter increases the linear density peak shifts radially outwards, indicating more volume is delivered at extreme radial locations, reflecting a greater contribution from large drops. In contrast, pressure has little effect on the

dimensionless volume density distribution as all four experimental conditions have similar shape.

Comparisons between the Basis, Tined, and Standard nozzles aligned with the tine (0º station) are provided in Figure 13(d) – (f) and comparisons between the three configurations aligned with the space (15º station) are depicted in Figure 13(g) – (i). Comparison of Figure 13(b), Figure 13(e) and Figure 13(h) reveal that the addition of tines in the Tined nozzle has little effect on the volume distribution when compared to the Basis nozzle with a similar orifice diameter. On the other hand, the addition of the boss in the Standard nozzle, Figure 13(f) and Figure 13(i), had a profound effect on the volume distribution throughout the spray when compared to the similar orifice diameters of the Basis nozzle, Figure 13(b), and Tined nozzle, Figure 13(e) and Figure 13(h). Also in contrast to the Tined and Basis nozzle, the volume density of the Standard nozzle depends significantly on the pressure, especially for measurements aligned with the tine (0º station).

3.4 Drop Size Distributions

Local drop size measurements were performed at 0.5 m stations spanning the entire sprinkler spray. The results are described in Figure 14 and summarized in Table 3 for all nozzle configurations and experimental conditions. Once again, the similarities between measurements from the Basis and Tined nozzles, Figure 14(a), are immediately apparent; whereas the spray from the Standard nozzle, Figure 14(b), behaves differently than the other configurations. For the Basis and Tined nozzles, the dimensionless location of drops passing through the measurement elevation is determined by the size of the drop. As drops travel from the deflector they are separated by drag effects in the air, resulting

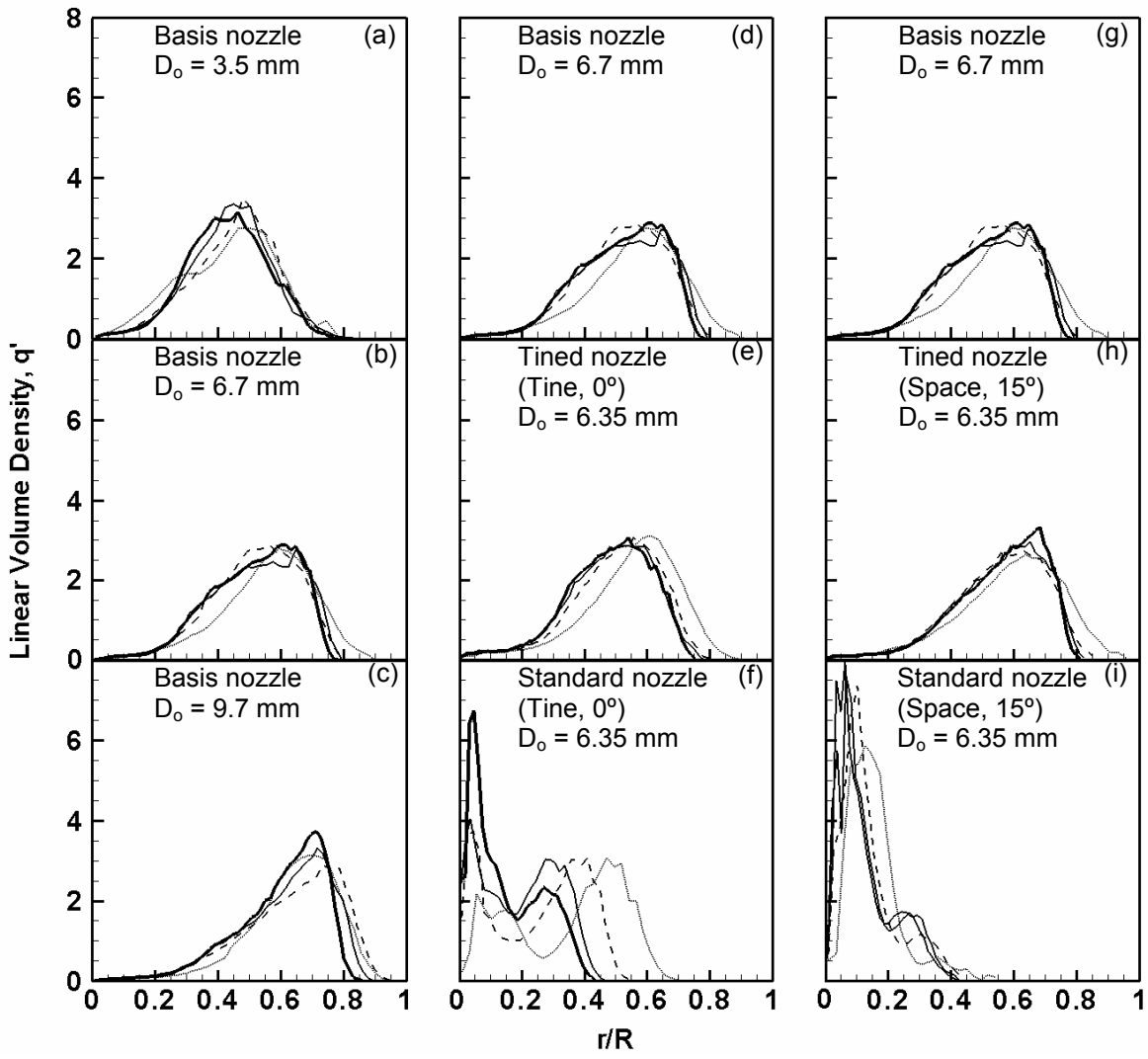

Figure 13. Volume Density measurements for all nozzle configurations and conditions: ····· 0.69 bar; - - - - 1.38 bar; —— 2.07 bar; ━━ 2.76 bar; Basis nozzle: (a) D_o = 3.5 mm, (b) D_o = 6.7 mm, (c) D_o = 9.7 mm, (d) D_o = 6.7 mm; Tined nozzle (Tine, 0º): (e) D_o = 6.35 mm; Standard nozzle (Tine, 0º): (f) D_o = 6.35 mm; Basis nozzle: (g) D_o = 6.7 mm; Tined nozzle (Space, 15º): (h) D_o = 6.35 mm; Standard nozzle (Space, 15º): (i) D_o = 6.35 mm.

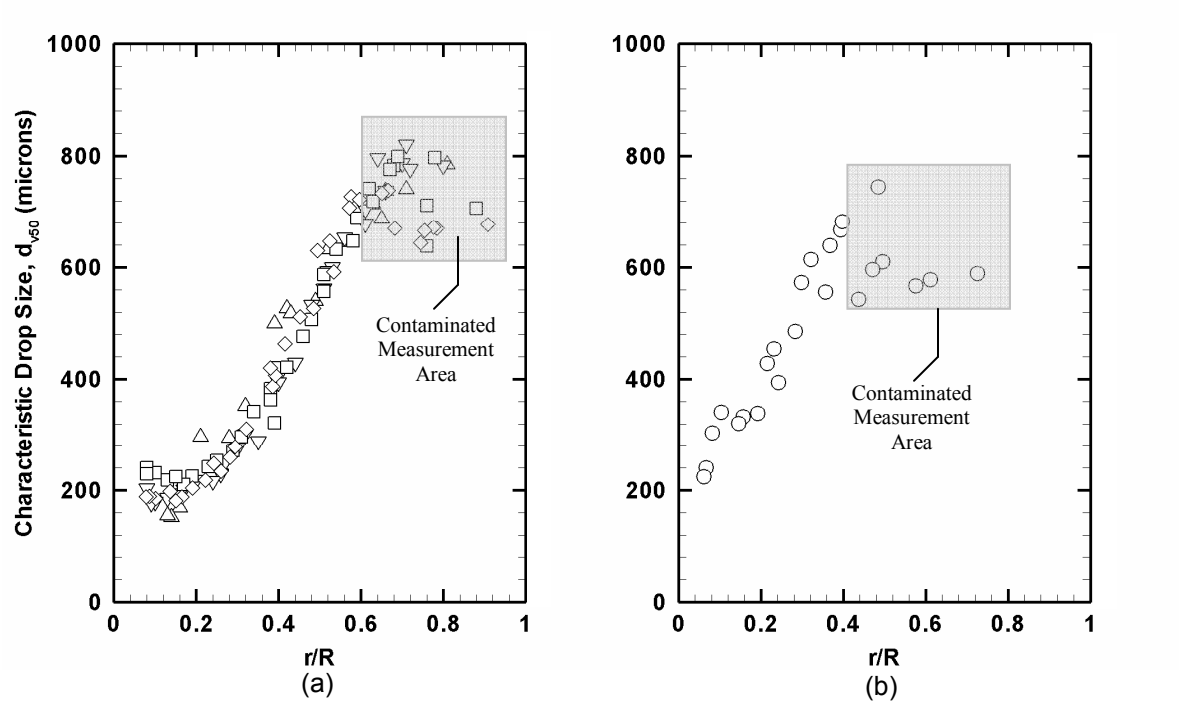

Figure 14. Local d_{v50} measurements for all nozzle configurations and conditions: (a) Basis nozzle: △ D_o = 3.5 mm; ▽ D_o = 6.7 mm; □ D_o = 9.7 mm; Tined nozzle (Tine, 0º): ◇ D_o = 6.35 m; (b) Standard nozzle (Tine, 0º): ○ D_o = 6.35 mm.

in smaller drops traveling shorter distances and larger drops traveling the furthest, as clearly seen in Figure 14(a). In contrast, with the addition of the boss in the Standard nozzle, larger drops appear much closer to the centerline, resulting from drops being formed by the flow of water directed through the spaces. This process creates a significantly different drop dispersion curve when compared to the Basis and Tined nozzles, as shown in Figure 14(a) and Figure 14(b).

When presenting drop size data, it is often useful to find overall spray characteristics for a given nozzle and experimental condition. The cumulative volume fraction is an extremely useful overall spray quantity describing the percentage of the total spray volume contained in drop sizes smaller than a specific drop diameter, for each nozzle and experimental condition. It has been shown that a Rosin-Rammler/log-normal drop size

distribution predicts the cumulative volume fraction for sprinkler sprays, which in turn is useful for modeling purposes [28]. The Rosin-Rammler/log-normal distribution is defined as

$$CVF = \begin{cases} (2\pi)^{-\frac{1}{2}} \int_0^{d_{CVF}} (w'd')^{-1} e^{-\frac{[\ln(d'/d_{v50})]^2}{2w'^2}} dd' & d_{CVF} \le d_{v50} \\ 1 - e^{-0.693(d_{CVF}/d_{v50})^w} & d_{v50} < d_{CVF} \end{cases} \tag{3.4}$$

where CVF is the cumulative volume fraction of drops with diameters less than d_{CVF}, w is a correlation coefficient, $w' = 2\left((2\pi)^{1/2}(\ln 2)w\right)^{-1} = 1.15/w$, found empirically. Figure 15(a) and Figure 15(b) provide sample drop size distributions for the Basis nozzle, D_o = 9.7 mm and the Standard nozzle at 2.07 bar, respectively. A Rosin-Rammler/log-normal equation curve fit to the cumulative volume fraction is also included to determine w,

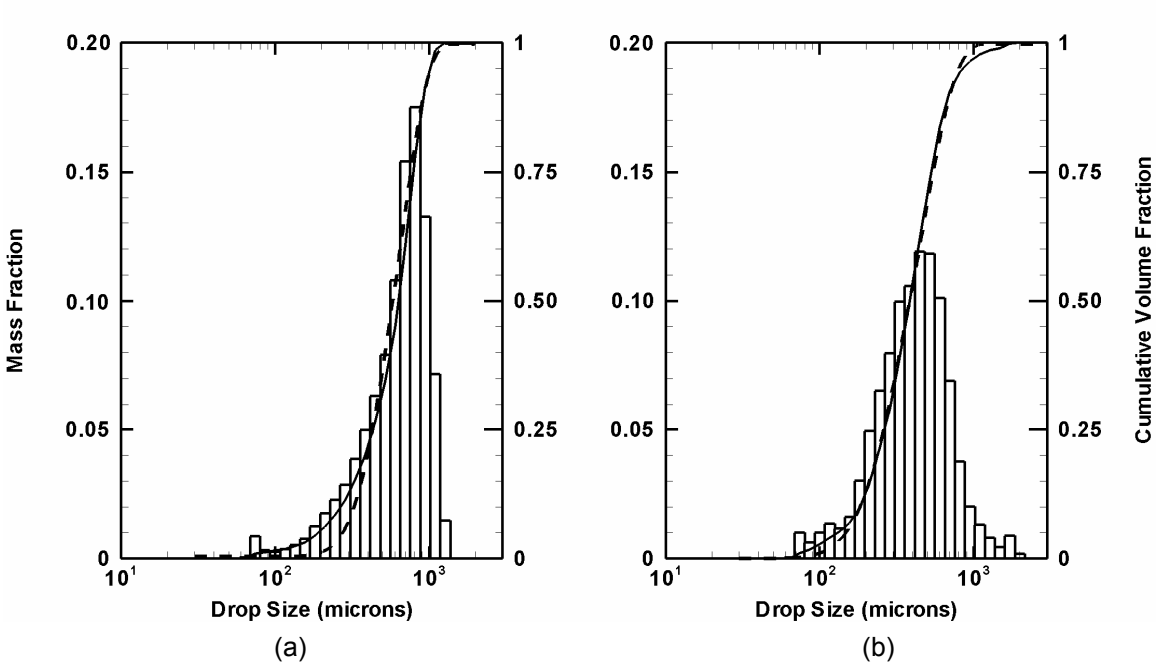

Figure 15. Drop size distribution at 2.07 bar: (a) Basis nozzle, D_o = 9.7 mm, (b) Standard nozzle, D_o = 6.35 mm; —— CVF; - - - Rosin-Rammler/log-normal.

yielding $w = 2.6$ with a $d_{v50} = 781$ μm for the Basis nozzle and $w = 2.0$ with a $d_{v50} = 393$ μm for the Standard nozzle. The agreement between the Standard nozzle and the Rosin-Rammler/log-normal distribution is very close, while the curve fit doesn't appear to predict the large number of smaller drops found in the Basis nozzle.

Although local drop size measurements are useful, the primary objective of these measurements was to determine an overall characteristic drop size, d_{v50}, for the entire spray. Dimensionless overall characteristic drop sizes, d_{v50}/D_o, for each experimental condition and nozzle configuration are presented in Figure 16 and have been summarized previously in Table 3. Similar to drop size results provided by Clanet and Villermaux [19] for a flat disk deflector configuration, the characteristic drop size for all three Basis

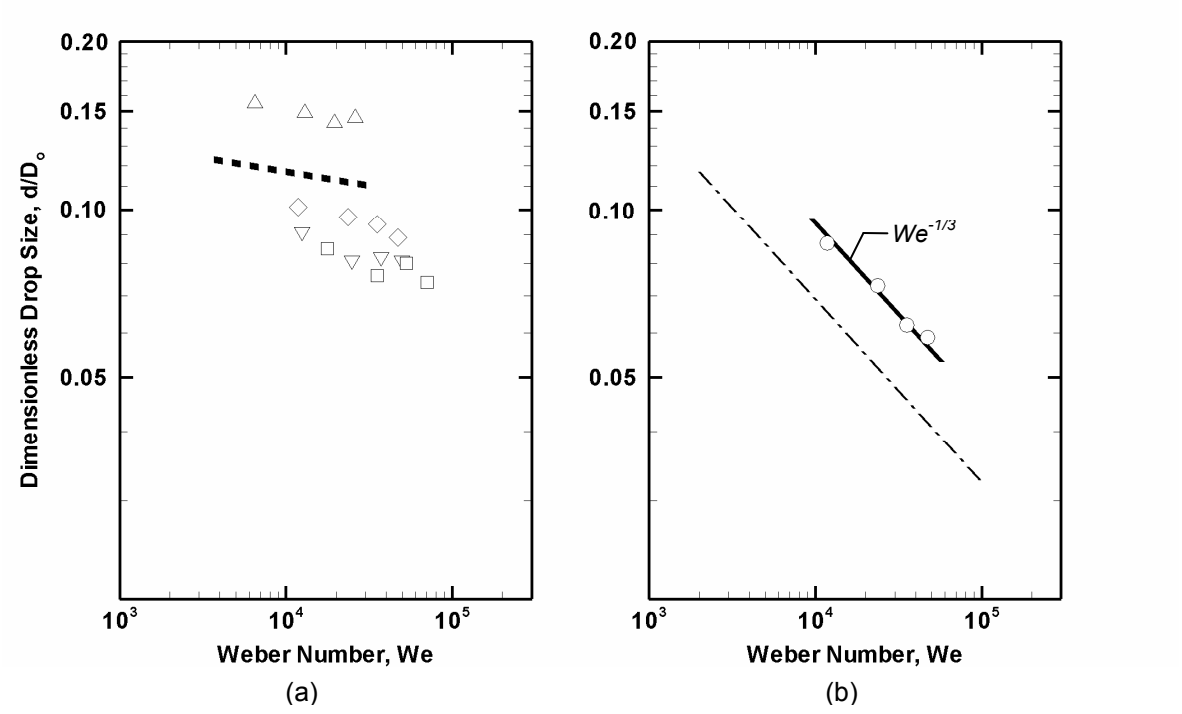

Figure 16. Experimental drop size results: (a) ▪▪▪▪ Clanet & Villermaux; Basis nozzle: △ D_o = 3.5 mm; ▽ D_o = 6.7 mm; □ D_o = 9.7 mm; Tined nozzle: ◇ D_o = 6.35 m; (b) Standard nozzle: ○ D_o = 6.35 mm; – · – Dundas Correlation; ▬ Standard Correlation.

nozzles shown in Figure 16(a) did not demonstrate a strong dependence on the Weber number. Following the same trend, the characteristic drop size measurements for the Tined nozzle, aligned with the tine (0º station), did not significantly differ from the Basis nozzle results. A very different trend is depicted in Figure 16(b), where the drop size measurements for the Standard nozzle aligned with the tine (0º station), followed the $We^{-1/3}$ scaling law proposed by Dundas [2] for sprinkler configurations. Dundas proposed the empirical correlation

$$d_{v50} / D_o = CWe^{-1/3} \tag{3.5}$$

shown in Figure 16(b), where $C = 1.41$, for the sprinkler configuration he tested. The constant, C, has been shown by Yu [3] and Sheppard [7], both testing a variety of commercially available sprinklers, to depend upon the sprinkler type. In this study, the experimental constant that best matched the drop size measurements was determined to be 2.04 for the Standard nozzle.

In addition to drop size measurements at locations aligned with the tine (0º station), measurements were also performed at locations aligned with the space (15º station). Overall drop size measurements for the Tined and Standard nozzles at each experimental condition have been included in Figure 17. The overall characteristic drop sizes from measurements of the Tined nozzle aligned with the space essentially have no Weber number dependence and are similar in drop diameter to the measurements aligned with the tine. However, drop size measurements from the Standard nozzle aligned with the space follow the expected $We^{-1/3}$ power law decay with considerably smaller drop sizes when compared to the measurements aligned with the tine. For the Standard nozzle the

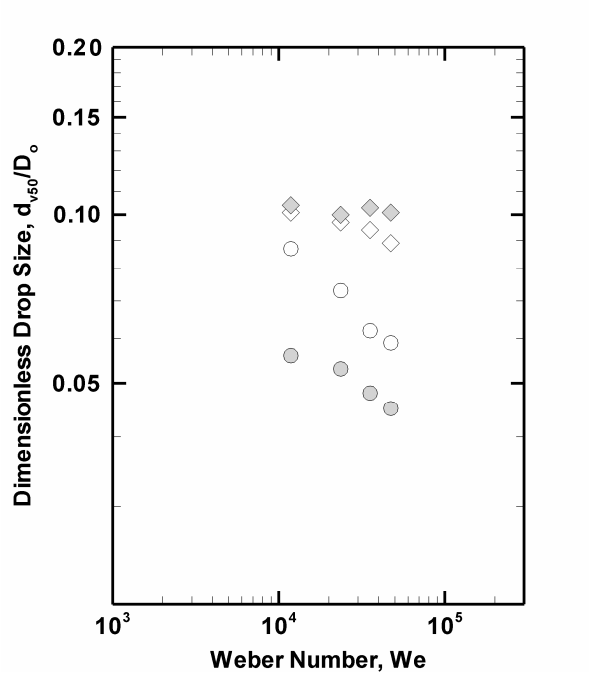

Figure 17. Dimensionless drop size results for spaces and tines: Tined nozzle: ◇ Tine (0º); ◆ Space (15º); Standard nozzle: ○ Tine (0º); ● Space (15º).

constant C from equation (3.5) when aligned with the space (15º station) was found to be $C = 1.48$.

Chapter 4: Conclusions

A series of experiments have been conducted to characterize the initial spray of canonical sprinkler configurations. Measurements were taken to determine the initial angle of the sheet as it exits the deflector, the distance the sheet travels before break-up, the volume and drop size distribution 1 meter below the sprinkler head.

The initial sheet angle exiting the deflector appears to be a function of the orifice diameter, and not pressure, where the initial angles fell in a range of 3.6º - 9.3º for the Basis nozzles with orifice diameters ranging from 3.5 mm – 9.7 mm. The addition of tines appeared to have a minimal impact on the initial angle of the sheet as it exits the deflector. However, the addition of a boss with tines in the Standard nozzle does appear to create a smaller average initial angle, 3.5º, when compared to the Tined nozzle, at 4.2º. Unfortunately, the trajectory of the water falling through the spaces of the tines could only be estimated qualitatively in this study.

The sheet breakup distances followed the previously proposed scaling law of $We^{-1/3}$ for the Basis and Standard nozzle with empirical correlations of $2r_{bu}/D_o = 964We^{-1/3}$ and $2r_{bu}/D_o = 495We^{-1/3}$, respectively. Similar to the initial angle measurements, the addition of tines on the deflector does not have a significant influence on the sheet breakup distance, unless a boss is also present.

The volume density distributions, when normalized by the characteristic dispersion length scale, *R,* did not vary significantly with an increasing Weber number for the Basis and Tined nozzles. Therefore, the addition of tines in a deflector did not have an effect on the volume distribution to the floor. However, with the addition of tines and a boss on the Standard nozzle, the volume density distributions were dramatically different than

those seen in the Basis and Tined nozzles. The volume density for the Standard nozzle saw significant amounts of water lost through the spaces at early radial locations, a characteristic not seen in the previous sprinkler configurations.

For the Basis and Tined nozzles, the characteristic drop sizes did not significantly change with respect to Weber number for a given configuration. This result, though unexpected, was in good agreement with the work of Clanet and Villermaux, who measured the drop size of an impinging jet configuration similar to this study's Basis nozzle. The Standard nozzle, the only commercially available nozzle tested, did follow the $We^{-1/3}$ scaling laws proposed by Dundas for sprinklers. This result suggests that the Basis nozzle, with its flat disk deflector, has unique and different Weber number functionality than what has been determined for conventional sprinklers. At this time it is not known which atomization mechanisms are responsible for this difference. With better diagnostics a more detailed look at the complex sheets produced by common sprinkler nozzles can be studied to determine those physical mechanisms.

References

[1] Grant, G., Brenton, J., and Drysdale, D., "Fire Suppression by Water Sprays," *Progress in Energy and Combustion Science*, Vol. 26, pp. 79-130, 2000.

[2] Dundas, P. H., "Technical Report Optimization of Sprinkler Fire Protection The Scaling of Sprinkler Discharge: Prediction of Drop Size," FMRC Serial No. 18792 RC73-T-40, *Factory Mutual Research Corporation*, Norwood, MA, June 1974.

[3] Yu, H. Z., "Investigation of Spray Patterns of Selected Sprinklers with the FMRC Drop Size Measuring System," *First International Symposium on Fire Safety Science,* New York, pp. 1165-1176, 1986.

[4] Widmann, J. F., Sheppard, D. T., and Lueptow, R. M., "Non-Intrusive Measurements in Fire Sprinkler Sprays", *Fire Technology*, Vol. 37, pp. 297-315, 2001.

[5] Widmann, J. F., "Phase Droppler Interferometry Measurements in Water Sprays Produced by Residential Fire Sprinklers", *Fire Safety Journal*, Vol. 36, pp. 545-567, 2001.

[6] Widmann, J. F., "Characterization of a Residential Fire Sprinkler using Phase Doppler Interferometry", NISTIR 6561, *National Institute of Standards and Technology*, Gaithersburg, MD, 2000.

[7] Sheppard, D. T., "Spray Characteristic of Fire Sprinklers," NIST GCR 02-838, *National Institute of Standards and Technology*, Gaithersburg, MD, 2002.

[8] Sheppard, D. T., Gandhi, P.D., "Understanding Sprinkler Sprays: Trajectory Analysis" NISTIR 6561, *National Institute of Standards and Technology*, Gaithersburg, MD, 2000.

[9] Putorti A. D., Belsinger T. D., and Twilley W. H., " Determination of Water Spray Drop Size and Speed from a Standard orifice, Pendent Spray Sprinkler", Report of Test. NIST, Gaithersburg, MD, May 1999.

[10] Putorti A.D., "Simultaneous Measurements of Drop Size and Velocity in Large-Scale Sprinkler Flow Using Particle Tracking and Laser-Induced Fluorescence", NIST GCR-861, *National Institute of Standards and Technology*, Gaithersburg, MD, 2004

[11] Fraser, R. P., Eisenklam, P., "Research into the Performance of Atomizers for Liquids", *Imp. Coll. Chem. Eng. Soc. J.*, Vol. 7, pp. 52-68, 1953.

[12] Dombrowski, N., Fraser, R. P., "Photographic Investigation into the Disintegration of Liquid Sheets", *Philos. Trans. R. Soc. London Ser. A, Math. Phys. Sci.*, Vol. 247, No. 924, pp. 101-130, 1954.

[13] Dombrowski, N., Hasson, D., Ward, D. E., "Some Aspects of Liquid Flow Through Fan Spray Nozzles", *Imp. Coll. Chem. Eng. Soc. J.*, Vol. 12, pp. 35-50, 1960.

[14] Dombrowski, N., Hooper, P. C., "The effect of Ambient Density on Drop Formation in Sprays", *Imp. Coll. Chem. Eng. Soc. J.*, Vol. 17, pp. 291-305, 1962.

[15] Huang, J. C., "The Break-up of Axisymmetric Liquid Sheets", *Journal of Fluid Mech.* Vol. 43, part 2, pp. 305-319, 1970.

[16] Arai, T., Hashimoto, H., "Disintegration of a Thin Liquid Sheet in a Cocurrent Gas Stream", *Proceesings of the 3rd International Conference on Liquid Atomization and Spray Systems*, London, 1985, pp. V1B/1/1-7.

[17] Prahl, J. M., Wendt, B., "Dishcharge Distribution Performance for an Axisymmetric Model of a Fire Sprinkler Head", *Fire Safety Journal*, Vol. 14, pp. 101-111, 1988.

[18] Clanet, C., Villermaux, E., "Life of a Smooth Liquid Sheet", *Journal of Fluid Mechanics*, Vol. 462, pp. 307-340, 2002.

[19] Villermaux, E., Clanet, C., "Life of a Flapping Liquid Sheet", *Journal of Fluid Mechanics*, Vol. 462, pp. 341-363, 2002.

[20] Weber, Z., *Angew Math Mech.* Vol.11 pp 136-154, 1931.

[21] Ostrach, A., Koestel, S., "Film instabilities in two-phase flows", *AIChE Journal*, Vol 11, pp. 294-303, 1965.

[22] Wu, D., Guillemin, D., Marshall, A.W., "A Modeling Basis for Predicting the Initial Sprinkler Spray", *Fire Safety Journal*, In Press, 2007.

[23] Wu, D., "Atomization Model for Fire Suppression Devices", *University of Maryland*, College Park, MD, 2005.

[24] Lefevre, A. H., "Atomization and Sprays" Indiana: Taylor and Francis, 1989.

[25] Crowe, C.T., Sommerfeld, M., and Tsuji, Y., "Multiphase Flows with Droplets and Particles", CRC Press, 1998, ISBN 0-8493-9469-4.

[26] Malvern Instruments/Insitec Inc., "Technical Specifications: EPCS", Issue 1.0, 1997.

[27] Krarup, A.,"Spraytec Cookbook: RTSizer software Vers. 5.1 to 5.3", Version 1.3, 2002.

[28] Chan, T.S., "Measurements of Water Density and Droplet Size Distributions of Selected ESFR Sprinklers", *Journal of Fire Protection Engineering*, 6(2):79–87, 1994.

[29] Lawson J. R., Walton W. D., and Evans, D. D., " Measurement of Droplet Size in Sprinkler Sprays", National Bureau of Standards, U.S. Department of Commerce, NBSIR 88-3715, Gaithersburg, MD, Feb. 1988.

[30] Jackman. L. A., Nolan P. F., Morgan H. P. "Characterization of Water Drops from Sprinkler Sprays", Fire Suppression Research – First International Conference, Stockholm, Sweden, 1992.

[31] Chow W. K. Shek L. C., "Physical Properties of a Sprinkler Water Spray", Fire Mater, Vol. 17, pp. 279-292, 1993.

[32] Chan T. S., "Measurements of Water Density and Drop Size Distributions of Selected ESFR Sprinklers", Journal of Fire Prot Engr, Vol. 6, pp. 79-87, 1994.

[33] Reitz, R. D., and Bracco, F. V. "Mechanism of Atomization of a Liquid Jet", *Physics of Fluids*, Vol. 25, pp. 1730-1742, 1982.

[34] Marshall, A. W. and Guillemin, D., "An Analytical Model for Prediction Initial Spray Properties from Liquid Suppression Devices," *Workshop on Fire Suppression Technologies Proceedings*, Mobile, AL, 2003.

[35] Heskestad, G., "Proposal for Studying Interaction of Water Sprays with Plume in Sprinkler Optimization Program," Memorandum to C. Yao, June 16, 1972.

[36] Dombrowski, N. and Johns, W. R., "The Aerodynamics Instability and Disintegration of Viscous Liquid Sheets", *Chemical Engineering Science*, Vol.18, pp.203-214, 1963.

[37] McGrattan, K., "Fire Dynamics Simulator (Version 4) Technique Reference Guide", *NIST Special Publication 1018*, 2004.

[38] Watson, E. J., "The Radial Spread of a Liquid Jet over a Horizontal Plane", *Journal of Fluid Mechanics*, Vol. 20, pp.481-499, 1964.

[39] Ibrahim, E. A., and Przekwas, A. J., "Impinging Jets Atomization", *Physics of Fluids A*, Vol. 3, pp. 2981, 1991.